APL MATERIALS **6**, 026602 (2018)

Monoclinic structures of niobium trisulfide

Matthew A. Bloodgood,[1] Pingrong Wei,[1] Ece Aytan,[2] Krassimir N. Bozhilov,[3] Alexander A. Balandin,[2] and Tina T. Salguero[1,a]
[1]*Department of Chemistry, University of Georgia, Athens, Georgia 30602, USA*
[2]*Nano-Device Laboratory (NDL) and Phonon Optimized Engineered Materials (POEM) Center, Department of Electrical and Computer Engineering, University of California–Riverside, Riverside, California 92521, USA*
[3]*Central Facility for Advanced Microscopy and Microanalysis, University of California–Riverside, Riverside, California 92521, USA*

(Received 19 September 2017; accepted 30 October 2017; published online 22 December 2017)

Two new polymorphs of niobium trisulfide are established by single crystal x-ray diffraction. NbS_3-IV crystallizes in the monoclinic space group $P2_1/c$ with lattice parameters a = 6.7515(5) Å, b = 4.9736(4) Å, c = 18.1315(13) Å, and β = 90.116(2)°. Its structure is based on chains of [NbS_6] trigonal prisms containing Nb–Nb pairs with a bond length of 3.0448(8) Å; this pairing causes the chains to corrugate slightly along their axis, a feature also present in triclinic NbS_3-I that leads to semiconductor properties. The stacking arrangement of chains is different in these polymorphs, however, with NbS_3-I having an ABCDE repeating sequence of chain bilayers and NbS_3-IV having an AB repeating sequence. HRTEM studies show the presence of topotactically-oriented intergrown zones and numerous dislocations, which result in mosaic structuring. A second new polymorph, NbS_3-V, crystallizes in the monoclinic space group $P2_1/m$ with lattice parameters a = 4.950(5) Å, b = 3.358(4) Å, c = 9.079(10) Å, β = 97.35(2)°. In contrast to NbS_3-IV, NbS_3-V maintains fixed a Nb–Nb bond distance of 3.358(4) Å along the chains, and it has an ABCDE repeating sequence of chain bilayers similar to NbS_3-I. High resolution scanning transmission electron microscopy (HR-STEM) imaging of an exfoliated NbS_3-V nanoribbon shows the continuous [NbS_6] chains oriented along the b-axis. These results provide the first firmly established structural data for monoclinic NbS_3. In addition, SEM images show the formation of NbS_3 rings and cylinders, and a combination of powder x-ray diffraction and Raman spectroscopy provides a way to distinguish between NbS_3 polymorphs. https://doi.org/10.1063/1.5005813

Many classes of materials have been proposed as replacements for semiconductor-based electronics technology as it progresses in complexity and miniaturization.[1] Transition metal chalcogenides are leading candidates in the current "beyond-graphene" milieu.[2] Metal dichalcogenide (MX_2) and trichalcogenide (MX_3) compositions, together with their polymorphs and alloys, provide a diverse set of materials exhibiting low dimensionality,[3–5] wide ranging electrical properties,[6–9] and reasonable processing options.[10,11] In recent work, we and others have investigated nanostructured MX_3 materials for electronic device applications.[6,7,9,12,13] The unique properties of these materials result from their dual low-dimensional nature, i.e., quasi-one-dimensional and two-dimensional (Q1D-2D). Their primary structural unit is the [MX_6] trigonal prism, which is fused end-to-end into continuous chains; this motif leads to quasi-one-dimensional electronic character as well as distinct anisotropy. Additional metal-chalcogenide interactions between neighboring chains result in bilayer sheets that can be flat (e.g., $ZrSe_3$) or corrugated (e.g., $TaSe_3$). These two-dimensional sheets, stacked and held together by van der Waals bonding, then make up the three-dimensional structure. Depending on the

[a]salguero@uga.edu

composition, structure, and morphology of any particular MX_3 sample, either one- or two-dimensional character may dominate. Much like MX_2 materials, MX_3 materials are amenable to mechanical or chemical exfoliation along the van der Waals gap,[6,14] and recent studies show that their properties can be maintained or even enhanced by nanostructuring.[12,15]

Here we consider NbS_3, arguably the least-well-understand metal trichalcogenide. The niobium–sulfur system contains a rich cornucopia of phases, including an unknown number of NbS_3 polymorphs, varying compositions from NbS to $Nb_{21}S_8$, and the possibility of non-stoichiometric phases.[16–19] Offsetting this complexity and piquing our interest are intriguing reports about the electrical and charge density wave (CDW) properties of certain NbS_3 samples, including multiple CDW transitions and room temperature charge transport.[3,20,21] However, further progress has been impeded by the absence of well-established structural information, spectroscopic characterization, or even reproducible synthetic details. Therefore, in this contribution, we aim to clarify the polymorphism of NbS_3 as part of the foundation required to understand its electronic properties.

To date, NbS_3 has been reported to crystallize in four forms: types I, II, III, and a high-pressure phase (Table I). Jellinek and co-workers first proposed a monoclinic $ZrSe_3$-type NbS_3 structure in 1960.[16] They reported a definitive structure in 1978, using single crystal x-ray diffraction data to refine the NbS_3 structure with a triclinic unit cell (notably having $\alpha = \gamma = 90°$).[22] This polymorph is known as NbS_3-I in the literature. Compared to other MX_3 structures, NbS_3-I has several unique features. The most remarkable feature is Nb–Nb pairing along the NbS_3 chain axis that manifests as alternating Nb–Nb bonds (~3.0 Å) and gaps (~3.7 Å). This linear Peierls distortion at room temperature causes NbS_3-I to be semiconducting, with an experimentally determined bandgap in the range of 0.66–1 eV (based on transport, optical transmittance, and photoconduction measurements), rather than metallic.[23–27] Another consequence is the doubling of the *b*-axis (6.730 Å) compared to other MX_3 structures (typically ~3.3 Å), which is needed to accommodate Nb–Nb pairs in the unit cell (Fig. 1). A recent report by Fedorov and co-workers demonstrated the solution-based exfoliation of NbS_3-I into nanoribbons.[11]

TABLE I. Unit cell and synthesis parameters for previously reported NbS_3 polymorphs as well as new polymorphs NbS_3-IV and NbS_3-V.

Polymorph	Synthesis conditions	Space group	Unit cell parameters		Z	Nb···Nb (Å)	References
			a, b, c, (Å)	α, β, γ (deg)			
NbS_3-I	NbS_2Cl_2; 588 → 569 °C, 48 h; slow cool	$P\bar{1}$	4.963 6.730 9.144	90 97.17 90	4	3.045 3.702	22
NbS_3-HP	Nb + S; 700 °C at 2 GPa, 0.5 h	$P2_1/m$	9.68 3.37 14.83	90 109.9 90	6	3.370	29
NbS_3-II (proposed)	Nb + S; 600 → 580 °C, 15 days	$P2_1/m$	9.9 3.4 18.3	90 97 90	...	...	26 and 27
NbS_3-II (proposed)	Nb + S; 500 °C	...	9.1–9.6 18.7–19.9 3.4	90 97–98 90	8	...	25
NbS_3-III (proposed)	NbS_2 + S; 550 °C, 21 days, 400 °C 48 h, air quench	...	~5 ... ~9	90 98–99 90	...	...	20
NbS_3-IV	Nb + S, I_2 transport; 670 → 570 °C, 10 days	$P2_1/c$	6.7515(5) 4.9736(4) 18.1315(13)	90 90.116(2) 90	4 (8)	3.0448(8) 3.7087(8)	This work
NbS_3-V	Nb + S, 10% S transport; 700 → 670 °C, 10 days	$P2_1/m$	4.950(5) 3.358(4) 9.079(10)	90 97.35(2) 90	2	3.358(4)	This work

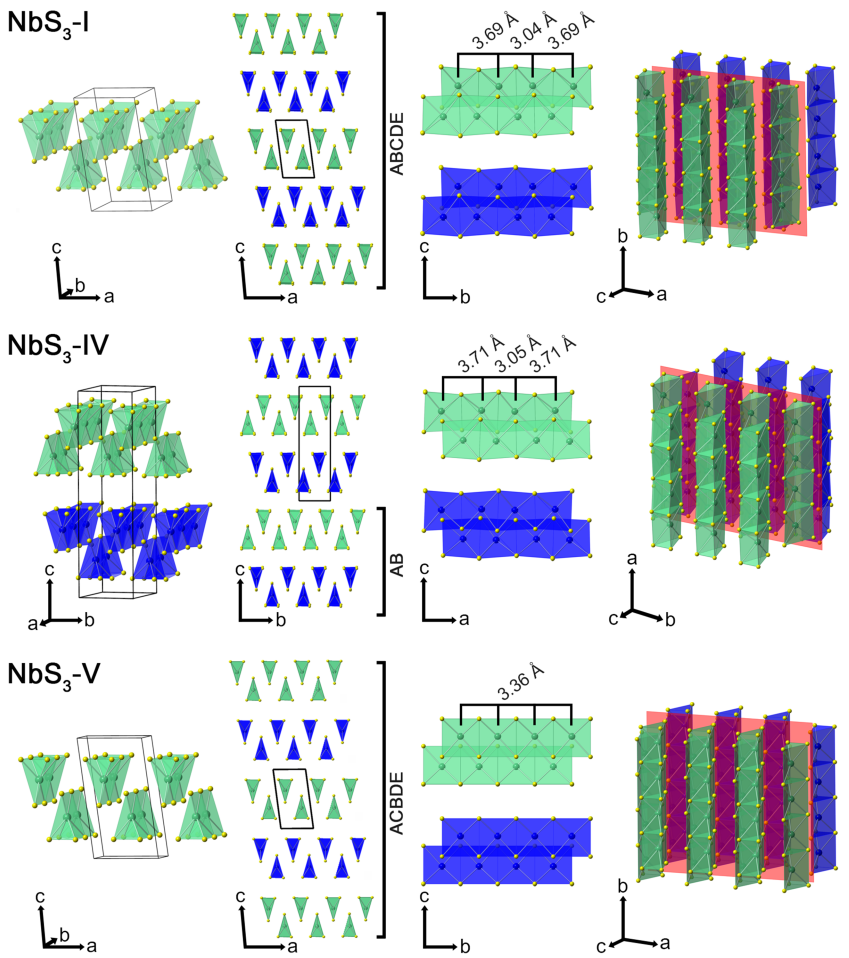

FIG. 1. Views of NbS_3-I, IV, and V: from left to right including unit cell, chain cross section, layer, and perspective views. The NbS_3 bilayers are differentiated by color to illustrate the van der Waals gaps, which is further illustrated with a red plane in each perspective view. The structures of these three polymorphs have been established by single crystal x-ray diffraction.

A second polymorph, NbS_3-II, was identified in 1978 based on electron diffraction studies, which showed inter-row pairs of satellite diffraction lines that resolved into rows of spots with varying temperature.[28] These rows occurred at irrational positions with similar separations as NbS_3-I, leading to the proposal that NbS_3-II was a superstructure of NbS_3-I with different chain stacking. Several years later, Prodan and co-workers introduced a model monoclinic NbS_3-II unit cell with lattice parameters $2a', b'/2, 2c', \beta'$ based on the NbS_3-I unit cell (lattice parameters a, b, c, β) (Table I).[29,30] In parallel, Roucau and co-workers proposed a closely related model monoclinic NbS_3-II unit cell with lattice parameters $2a'', 2c'', b''/2, \beta''$ based on a different multiple of the NbS_3-I unit cell (Table I).[26,31,32] In the almost forty years since NbS_3-II was identified, however, its atomic structure has remained unsolved. During this time, continued interest in this polymorph has been motivated by its three CDWs: a low temperature transition at 150 K, a second transition at 330-370 K, and a high temperature transition at 620-650 K.[21,26] The transition at 330-370 K, just above room temperature, is an unusual one for CDW transport, and according to Zybtsev and co-workers, this CDW exhibits high transport velocities and sliding coherence.[21]

A high-pressure modification of NbS_3 prepared at 700 °C with 2 GPa pressure was reported by Kikkawa and co-workers in 1982.[33] The monoclinic unit cell deduced from powder x-ray diffraction data is similar to that of monoclinic $NbSe_3$ (Table I), but atomic positions for NbS_3-HP could not be determined.[33] Yet another polymorph, designated NbS_3-III, was reported by Zettl

and co-workers in 1982. In this case, powder x-ray diffraction data provided only partial lattice parameters. However, NbS_3-III can be distinguished by a characteristic CDW transition at 155 K.[20] Subsequent electrical measurements by Zybtsev and co-workers on "low-ohmic" and "high-ohmic" NbS_3 samples showed that low-ohmic NbS_3 exhibits CDW transitions at both 150 and 360 K, whereas high-ohmic NbS_3 exhibits a single CDW transition at 150 K.[3] On this basis, it has been postulated that low-ohmic and high-ohmic NbS_3 correspond to NbS_3-II and NbS_3-III, respectively; an alternate interpretation is that low- and high-ohmic NbS_3 as well as NbS_3-III are sub-phases of NbS_3-II.[21]

This letter reports the growth and characterization of two new monoclinic polymorphs of NbS_3, designated NbS_3-IV and NbS_3-V following the nomenclature currently in place. Interestingly, we isolated NbS_3-IV under synthetic conditions previously reported to produce NbS_3-I and NbS_3-V under synthetic conditions previously reported to produce NbS_3-II.[3,34] Single crystal x-ray diffraction studies of both NbS_3-IV and NbS_3-V provide unambiguous structural information about these polymorphs. Such definitive characterization is necessary for accurate identification, especially because NbS_3 polymorphs form under similar conditions and often more than one can be found in the same crystal growth batch.[28] Furthermore, electron microscopy analysis provides information about structural defects in NbS_3-IV and atomic order in NbS_3-V, and Raman spectroscopy of NbS_3-IV and NbS_3-V provides data that can be used to distinguish between polymorphs.

Niobium trisulfide samples were synthesized using niobium powder (99.99%, STREM) and sublimed sulfur powder (Baker, >99%) using a chemical vapor transport method. Iodine (Baker, 98%) at 4–6 mg/cm^3 was used for the growth of the NbS_3-IV phase, whereas excess sulfur (~10%) was utilized as the transport agent for the growth of NbS_3-V crystals. For all syntheses, niobium and sulfur were lightly ground by mortar and pestle before being placed in a quartz ampule (~13 cm^3). The ampules were then evacuated and backfilled with argon three times before flame sealing under vacuum (~10^{-2} Torr). Reactions were placed in a two-zone furnace with a fixed gradient for 10–14 days; upon completion, the ampule/furnace was allowed to cool to room temperature naturally.

NbS_3-IV crystals used for x-ray diffraction analysis were prepared at 670 °C with a 100 °C gradient (670 °C source zone → 570 °C growth zone). This synthesis temperature is comparable to temperatures used to prepare NbS_3-I,[11,27,34] and the only difference here is the use of I_2 as a transport agent. This NbS_3 polymorph crystallizes in a monoclinic unit cell, and the structure was solved using space group $P2_1/c$. Additional details are provided in Tables S1 and S2 of the supplementary material, and crystallographic data have been deposited with the Cambridge Crystallographic Data Centre (structure number 1574381).

The unit cell of NbS_3-IV is larger than that of NbS_3-I because the *c*-axis is doubled, resulting in twice as many chains per unit cell (Fig. 1). The asymmetric unit of NbS_3-IV is Nb_2S_6, making Z formally 4, which becomes 8 when normalized to the formula NbS_3. Also, in contrast to other MX_3 structures, the chain axis in NbS_3-IV is the *a*-axis rather than the *b*-axis (Fig. 1). Looking down the *a*-axis, the structure of NbS_3-IV in cross section is similar to the model $ZrSe_3$-type structure, specifically the "A-variant."[35] However, a difference between these structures is their layer-stacking order. This is clearly seen when examining multiple unit cells of each polymorph (Fig. 1). The chains in NbS_3-I realign every five bilayers, where a bilayer is defined as a pair of chains bounded by van der Waals gaps (Fig. 1 where pairs of blue or green chains designate the bilayers). Thus, the repeat sequence is ABCDE. However, NbS_3-IV experiences a realignment of the chain after only two bilayers, making the repeat sequence AB.

In the chain cross section of NbS_3-IV, three sulfur atoms surround a niobium atom to form acute, isosceles triangles. The bases of the triangles are made of a 2.015 Å S–S bond; the presence of this bond is consistent with the formulation of NbS_3 as $Nb(S_2)S$.[22] The sides of the triangles are separated by longer S···S distances of 3.404-3.418 Å or 3.787-3.828 Å. Two interchain Nb–S bonds of 2.623 and 2.654 Å exist between each chain, which hold the bilayer together. Each bilayer is separated from the next by a distance of ~2.8 Å, the van der Waals gap.

Looking down the *b*-axis (Fig. 1), we see that NbS_3-IV contains Nb–Nb pairing with a bond distance of 3.0448 Å, much like NbS_3-I. Thus, NbS_3-IV demonstrates that it is possible to have Nb–Nb pairing within a space group with $P2_1/c$ symmetry, i.e., it is not essential to reduce the

symmetry to triclinic as in NbS_3-I. It is curious that Jellinek and co-workers published two papers prior to their report of NbS_3-I's triclinic structure in which they reported monoclinic unit cells extremely similar to what we have found for NbS_3-IV.[16,17] It is possible that they actually made NbS_3-IV in earlier work, which was based on the synthesis of NbS_3 from the elements, whereas their structural study was conducted on NbS_3 crystals generated through the thermal decomposition of NbS_2Cl_2.[22] The differences in preparative conditions may have led to the formation of NbS_3-I versus NbS_3-IV. In addition, van Smaalen has re-interpreted the triclinic space group $P\bar{1}$ of NbS_3-I as a monoclinic superspace group, proposing that this is an uncommon example of a modulated structure.[36]

The relatively high *wR* value (11.38%) associated with the refinement of NbS_3-IV reflects the presence of structural disorder, possibly including sulfur vacancies, faulting or slippage along the van der Waals planes, and twinning, all of which have been observed in various MX_3 materials.[28,35,37] To identify the specific disorder in NbS_3-IV, the TEM analysis was performed on a Thermo Fisher Scientific Themis 300 instrument, fitted with a X-FEG electron gun and CETA 4K × 4K CMOS camera, at an accelerating voltage of 300 kV. Specimens were prepared by dispersing a small amount of as-synthesized NbS_3-IV powder in distilled water without grinding and depositing a droplet of the resulting suspension onto lacey carbon grids. The TEM study revealed that the sample consists of three types of particles: (1) long thin whiskers with aspect ratios >100 and thicknesses <100 nm that are elongated parallel to the *a*-axis [Fig. 2(a)]; (2) prismatic crystals with aspect ratios <20, with a long side parallel to the *a*-axis, a short side parallel to the *b*-axis, and thicknesses <100 nm along the *c*-axis [Fig. 2(b)]; (3) small aggregates consisting of isometric particles <50 nm in diameter.

The fibers of NbS_3-IV are twisted around their long axis, resulting in the development of numerous dislocations that can be identified through disruptions of the lattice fringes parallel to {001} [Fig. 2(a)]. The prismatic particles consist of topotactically intergrown zones 5–50 nm wide parallel to the *b*-axis and several microns long parallel to the *a*-axis [Fig. 2(b)]. They are coherently intergrown with interfaces parallel to the {010} planes. The individual crystals exhibit a mosaic structure with fine domains about 10 nm in diameter [Fig. 2(c)] that are coherently intergrown with small angular mis-orientation around the *c*-axis, which cause changes in the contrast and appearance of the lattice fringes resolved by HRTEM imaging. It is possible that the observed variations in the lattice images along the *c*-axis are caused by stacking defects; it is possible to resolve such features by imaging down the *a*-axis, but this has not been done here due to the unfavorable particle shapes.

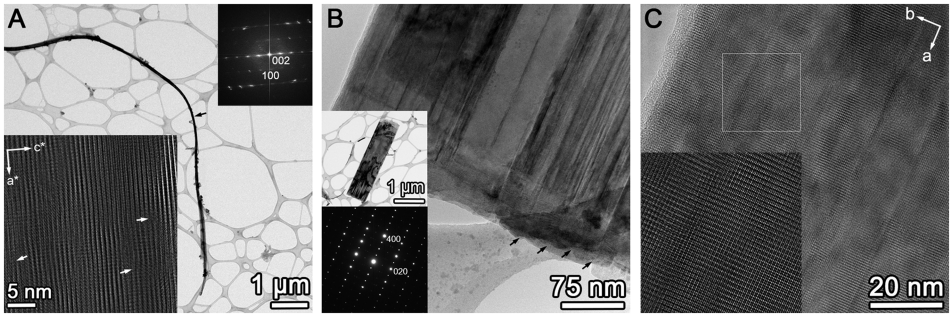

FIG. 2. (a) Bright field TEM image of a NbS_3-IV fiber. Insets show (i) HRTEM image (lower left) of the crystal along the *b*-axis and (ii) the corresponding indexed FFT pattern (upper right). The location of the HRTEM image is indicated by a black arrow. In the HRTEM inset, multiple disruptions of the lattice fringes parallel to {001} are visible; some dislocations are indicated by white arrows. (b) Bright field high magnification TEM image of a prismatic NbS_3-IV particle. Insets shown are (i) low magnification BF TEM image of the whole particle (upper) and (ii) the corresponding selected area electron diffraction pattern along the c-axis, which confirms the single crystal nature of the whole particle. The topotactically oriented individual intergrown zones are clearly visualized, with some of the coherent interfaces between zones indicated by black arrows. (c) HRTEM image of the particle in (b). The inset shows a magnified view of the area marked by a white box. The complex lattice contrast and the mosaic structure of low-angle domains is revealed here; the slight tilt of the domains causes considerable change in the lattice fringe contrast, which prevents the reliable interpretation of any stacking disorder that might be present parallel to the *c*-axis.

Further exploration of the NbS_3 system provided yet another monoclinic NbS_3 polymorph, NbS_3-v. It was prepared at 700 °C with a 30 °C gradient (700 °C source zone → 670 °C growth zone) using 10% excess sulfur for transport. This polymorph also crystallizes in the $P2_1/m$ space group. Additional details are provided in Tables S1 and S2 of the supplementary material, and crystallographic data have been deposited with the Cambridge Crystallographic Data Centre (structure number 1574382). As illustrated in Fig. 1, the unit cell of NbS_3-v is similar to that of NbS_3-I but with a halved *b*-axis; the lattice parameters can be expressed as a', $b'/2$, c', β' based on the NbS_3-I unit cell (Table I). These dimensions result in two chains per unit cell, albeit the unit cell is only one $[MX_6]$ trigonal prism wide ($Z = 2$). This unit cell is smaller than those proposed for NbS_3-II.

In the chain cross section of NbS_3-v, three sulfur atoms surround a niobium atom to form acute isosceles triangles with bases composed of 2.020 Å S–S bonds and sides formed by S···S distances of 3.576-3.612 Å. Interestingly, the interchain Nb–S interactions alternate in pairs of 2.619 Å and 2.635 Å Nb–S bonds, which results in a small but measurable chain pairing within the bilayer sheet. Although NbS_3-v features the same ABCDE stacking that occurs in NbS_3-I (Fig. 1), it contains a single, uniform Nb–Nb distance of 2.358 Å, leading to ideal (non-corrugated) $[MX_6]$ chains. Theoretically, NbS_3 with such an undistorted structure should display metallic conductivity due to a single electron remaining on each Nb^{4+} after creation of the $[NbS_6]$ chains.[23,38]

NbS_3-IV and NbS_3-v can be exfoliated in a similar fashion as other MX_3 materials.[5,6,13] Figure 3 shows HAADF-STEM images of a ~40 nm wide NbS_3-v nanoribbon exfoliated by sonication in ethanol. The high-resolution image in panel (b) reveals the $[NbS_6]$ chains along the *b*-axis. Both the Nb–Nb bonds with 3.37 Å spacing and the van der Waals gap between chains are clearly visible. There are no defects visible at this magnification in this particular area of the sample or others imaged along this nanoribbon, although the high *wR* value (21.99%) associated with the refinement of NbS_3-v points to the presence of significant structural disorder in the larger crystal used for x-ray diffraction analysis.

In experimental material research, powder x-ray diffraction (PXRD) is usually the initial characterization method used to identify crystalline phases and evaluate phase purity. The patterns for NbS_3-I, IV, and v are compared in Fig. 4(a). Although the theoretical patterns (calculated from single-crystal XRD structures) of NbS_3-I and NbS_3-IV are similar, each has distinct peaks in the range 10°-40° 2θ that should make polymorph identification unambiguous. In practice, however, the experimental peak intensities of NbS_3-IV (powder mount) are altered by orientation effects, such that the resulting pattern can be matched to either NbS_3-I or NbS_3-IV. In the case of NbS_3-v, its theoretical pattern is essentially identical to that of NbS_3-I, but experimentally NbS_3-v powder generates a distinct pair of peaks at ~22° 2θ. Thus, we caution that PXRD alone is not sufficient to differentiate between all NbS_3 polymorphs.

Raman spectroscopy provides additional data to differentiate NbS_3-IV and NbS_3-v. As shown in Fig. 4(b), the spectra of these polymorphs are clearly different. However, the spectrum of NbS_3-v is not as clearly resolved as that of NbS_3-IV, which may be due to the structural disorder present. The spectrum of NbS_3-IV is similar but not identical to data published for NbS_3-I.[11,39–41] The specific differences are (1) the relative intensities of the two peaks at 145-155 nm are switched and (2) the

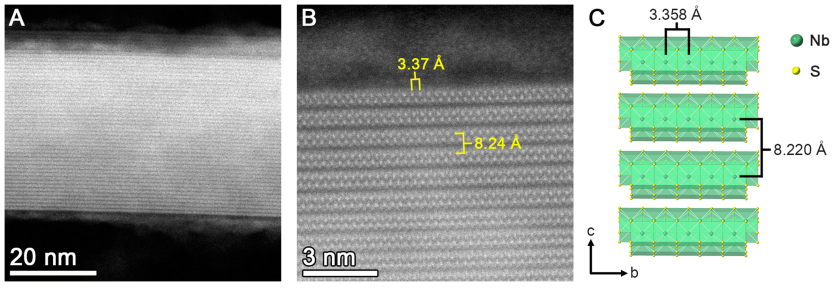

FIG. 3. HAADF-STEM images of an exfoliated NbS_3-v nanoribbon along the *b*-axis at low (a) and high magnifications (b), together with a structural model for the observed atomic spacings (c).

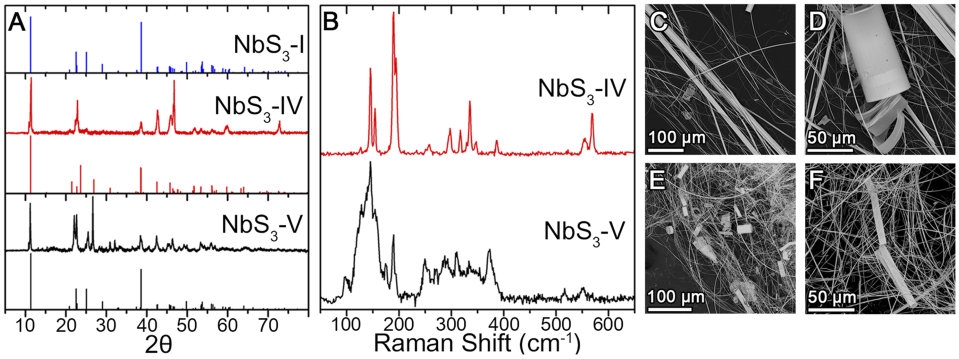

FIG. 4. (a) Powder x-ray diffraction patterns of NbS_3-I, NbS_3-IV, and NbS_3-V; drop lines for NbS_3-I are from JCPDS card no. 04-007-1130. Powder x-ray diffraction data for NbS_3-IV, and NbS_3-V were collected on a Bruker Advance D8 diffractometer with Co-Kα radiation at 35 kV and 40 mA from 5° to 80° 2θ with a 0.01 step size at 0.4 s/step. (b) Raman spectroscopy of NbS_3-IV and NbS_3-V. Raman data were collected on a Renishaw InVIA microscope at 785 nm with a 50× objective lens. SEM images of NbS_3-IV [(c) and (d)] and NbS_3-V [(e) and (f)]. SEM was conducted on a FEI Teneo FE-SEM instrument equipped with an Oxford Instruments X-MAX^N detector at 5–20 keV.

literature spectra for NbS_3-I show a single peak at ∼190 nm [assigned as ν(Nb· · · S_2) in Ref. 38], whereas the spectrum of NbS_3-IV in Fig. 4(b) has two peaks at this position. This latter difference is reasonable based on the asymmetric unit of Nb_2S_6 in NbS_3-IV, which should lead to two distinct ν(Nb· · · S_2) modes.

SEM images [Figs. 4(c)–4(f)] show that the morphology of NbS_3-IV and NbS_3-V is fibrous. NbS_3-IV crystals generally appear as wider, straight fibers, whereas NbS_3-V crystals look more like flexible wires. These morphological observations are similar to descriptions of NbS_3-I (larger, straighter needles) and NbS_3-II (finer, bent whiskers) in the literature.[22,30,34] In addition to the fibers, both products contain numerous cylinders and rings in various stages of winding/unwinding [Figs. 4(d) and 4(e)]. Moreover, energy dispersive spectroscopy (EDS) analysis indicates that these microstructures have a NbS_3 stoichiometry identical to the fibers. Such "topological crystals," previously observed for TaS_3, $NbSe_3$, and $TaSe_3$, apparently form when droplets of molten elemental chalcogen template crystal growth.[42–46] Indeed, Enyashin and Ivanovskiĭ have provided a theoretical basis indicating that NbS_3 ring structures are energetically favorable.[47] Continuing work will be required to understand the formation mechanism of such morphologies in the NbS_3 system and characterize the distortions that accompany crystal bending.

In summary, the crystal structures of two new niobium trisulfide polymorphs, NbS_3-IV and NbS_3-V, greatly enrich our understanding of this system. Both polymorphs crystallize in monoclinic unit cells, which fills a long-standing gap of knowledge about monoclinic NbS_3. We find that the structure of NbS_3-IV is related to triclinic NbS_3-I with respect to Nb–Nb pairing along the chain axis. In comparison, the structure of NbS_3-V is undistorted along the chain axis but contains subtle chain pairing. This structural information will be extremely helpful for the interpretation of spectroscopic data and modeling the electronic properties of NbS_3-IV and NbS_3-V.

See supplementary material for additional information about the x-ray diffraction studies of NbS_3-IV and NbS_3-V, including atomic coordinates.

This work was supported by a U.S. National Science Foundation's Emerging Frontiers of Research Initiative 2-DARE Grant (No. NSF EFRI-1433395).

[1] A. Kuc, *Chemical Modelling: Volume 11* (The Royal Society of Chemistry, 2015), Vol. 11, p. 1.
[2] X. Song, Z. Guo, Q. Zhang, P. Zhou, W. Bao, and D. W. Zhang, Small **13**, 1700098 (2017).
[3] S. G. Zybtsev, V. Y. Pokrovskii, V. F. Nasretdinova, and S. V. Zaitsev-Zotov, Phys. B **407**(11), 1696 (2012).
[4] Y. S. Hor, Z. L. Xiao, U. Welp, Y. Ito, J. F. Mitchell, R. E. Cook, W. K. Kwok, and G. W. Crabtree, Nano Lett. **5**(2), 397 (2005).
[5] Y. Jin, X. Li, and J. Yang, Phys. Chem. Chem. Phys. **17**(28), 18665 (2015).
[6] M. A. Stolyarov, G. Liu, M. A. Bloodgood, E. Aytan, C. Jiang, R. Samnakay, T. T. Salguero, D. L. Nika, S. L. Rumyantsev, M. S. Shur, K. N. Bozhilov, and A. A. Balandin, Nanoscale **8**(34), 15774 (2016).

[7] G. Liu, S. Rumyantsev, M. A. Bloodgood, T. T. Salguero, M. Shur, and A. A. Balandin, Nano Lett. **17**(1), 377 (2017).
[8] A. Grisel, F. Lévy, and T. J. Wieting, Physica B+C **99**(1), 365 (1980).
[9] J. O. Island, M. Barawi, R. Biele, A. Almazán, J. M. Clamagirand, J. R. Ares, C. Sánchez, H. S. J. van der Zant, J. V. Álvarez, R. D'Agosta, I. J. Ferrer, and A. Castellanos-Gomez, Adv. Mater. **27**(16), 2595 (2015).
[10] P. A. Poltarak, S. B. Artemkina, A. I. Bulavchenko, T. Yu. Podlipskaya, and V. E. Fedorov, Russ. Chem. Bull. **64**(8), 1850 (2015).
[11] V. E. Fedorov, S. B. Artemkina, E. D. Grayfer, N. G. Naumov, Y. V. Mironov, A. I. Bulavchenko, V. I. Zaikovskii, I. V. Antonova, A. I. Komonov, and M. V. Medvedev, J. Mater. Chem. C **2**(28), 5479 (2014).
[12] J. O. Island, A. J. Molina-Mendoza, M. Barawi, R. Biele, E. Flores, J. M. Clamagirand, J. R. Ares, C. Sánchez, H. S. J. van der Zant, R. D'Agosta, I. J. Ferrer, and A. Castellanos-Gomez, 2D Mater. **4**(2), 022003 (2017).
[13] A. Lipatov, P. M. Wilson, M. Shekhirev, J. D. Teeter, R. Netusil, and A. Sinitskii, Nanoscale **7**(29), 12291 (2015).
[14] Z. Yan, C. Jiang, T. R. Pope, C. F. Tsang, J. L. Stickney, P. Goli, J. Renteria, T. T. Salguero, and A. A. Balandin, J. Appl. Phys. **114**(20), 204301 (2013).
[15] J. Wu, D. Wang, H. Liu, W. M. Lau, and L. Liu, RSC Adv. **5**, 21455 (2015).
[16] F. Jellinek, G. Brauer, and H. Muller, Nature **185**(4710), 376 (1960).
[17] F. Kadijk and F. Jellinek, J. Less-Common Met. **19**(4), 421 (1969).
[18] M. Kurdi, A.-M. Marie, and M. Danot, Solid State Commun. **64**(4), 395 (1987).
[19] A. V. Mishchenko, I. V. Yushina, and V. E. Fedorov, Zh. Neorg. Khim. **33**(2), 437 (1988).
[20] A. Zettl, C. M. Jackson, A. Janossy, G. Grüner, A. Jacobsen, and A. H. Thompson, Solid State Commun. **43**(5), 345 (1982).
[21] S. G. Zybtsev, V. Y. Pokrovskii, V. F. Nasretdinova, S. V. Zaitsev-Zotov, V. V. Pavlovskiy, A. B. Odobesco, W. Wu Pai, M. W. Chu, Y. G. Lin, E. Zupanič, H. J. P. van Midden, S. Šturm, E. Tchernychova, A. Prodan, J. C. Bennett, I. R. Mukhamedshin, O. V. Chernysheva, A. P. Menushenkov, V. B. Loginov, B. A. Loginov, A. N. Titov, and M. Abdel-Hafiez, Phys. Rev. B **95**(3), 035110 (2017).
[22] J. Rijnsdorp and F. Jellinek, J. Solid State Chem. **25**(4), 325 (1978).
[23] D. W. Bullett, J. Solid State Chem. **33**(1), 13 (1980).
[24] M. E. Itkis, F. Ya. Nad, S. V. Zaitsev-Zotov, and F. Lévy, Solid State Commun. **71**(11), 895 (1989).
[25] M. E. Itkis, F. Ya. Nad, and F. Levy, Synth. Met. **43**(3), 3969 (1991).
[26] Z. Z. Wang, P. Monceau, H. Salva, C. Roucau, L. Guemas, and A. Meerschaut, Phys. Rev. B **40**(17), 11589 (1989).
[27] V. Nasretdinova and S. Zaitsev-Zotov, Phys. B **407**(11), 1874 (2012).
[28] T. Cornelissens, G. Van Tendeloo, J. Van Landuyt, and S. Amelinckx, Phys. Status Solidi A **48**(1), K5 (1978).
[29] F. W. Boswell and A. Prodan, Physica B+C **99**(1), 361 (1980).
[30] A. Prodan, A. Budkowski, F. W. Boswell, V. Marinkov, J. C. Bennett, and J. M. Corbett, J. Phys. C: Solid State Phys. **21**(23), 4171 (1988).
[31] C. Roucau, J. Phys. Colloq. **44**(C3), C3 (1983).
[32] A. Meerschaut, J. Phys. Colloq. **44**(C3), C3 (1983).
[33] S. Kikkawa, N. Ogawa, M. Koizumi, and Y. Onuki, J. Solid State Chem. **41**(3), 315 (1982).
[34] V. Y. Pokrovskii, S. G. Zybtsev, M. V. Nikitin, I. G. Gorlova, V. F. Nasretdinova, and S. V. Zaitsev-Zotov, Phys.-Usp. **56**(1), 29 (2013).
[35] E. Guilmeau, D. Berthebaud, P. R. N. Misse, S. Hebert, O. I. Lebedev, D. Chateigner, C. Martin, and A. Maignan, Chem. Mater. **26**, 5585 (2014).
[36] S. van Smaalen, Phys. Rev. B **38**(14), 9594 (1988).
[37] N. B. Bolotina, I. G. Gorlova, I. A. Verin, A. N. Titov, and A. V. Arakcheeva, Crystallogr. Rep. **61**(6), 923 (2016).
[38] K. Endo, H. Ihara, K. Watanabe, and S.-I. Gonda, J. Solid State Chem. **39**(2), 215 (1981).
[39] C. Sourisseau, R. Cavagnat, M. Fouassier, and P. Maraval, J. Raman Spectrosc. **21**(6), 337 (1990).
[40] C. Sourisseau, R. Cavagnat, M. Fouassier, and P. Maraval, J. Mol. Struct. **219**, 183 (1990).
[41] A. Zwick, M. A. Renucci, R. Carles, N. Saint-Cricq, and J. B. Renucci, Physica B+C **105**(1), 361 (1981).
[42] S. Tanda, H. Kawamoto, M. Shiobara, Y. Sakai, S. Yasuzuka, Y. Okajima, and K. Yamaya, Phys. B **284-288**(Part 2), 1657 (2000).
[43] T. Matsuura, S. Tanda, K. Asada, Y. Sakai, T. Tsuneta, K. Inagaki, and K. Yamaya, Phys. B **329-333**(Part 2), 1550 (2003).
[44] T. Tsuneta and S. Tanda, J. Cryst. Growth **264**(1-3), 223 (2004).
[45] G. Kumagai, T. Matsuura, K. Ichimura, and S. Tanda, Phys. B **405**(Suppl. 11), S284 (2010).
[46] M. Tsubota, K. Inagaki, T. Matsuura, and S. Tanda, Cryst. Growth Des. **11**(11), 4789 (2011).
[47] A. N. Enyashin and A. L. Ivanovskiĭ, Phys. Solid State **48**(4), 780 (2006).